Layer-by-layer Assembly of Nanocomposites for Energy Applications

by

Szushen Ho

A dissertation submitted in partial fulfillment
of the requirements for the degree of
Doctor of Philosophy
(Chemical Engineering)
in The University of Michigan
2011

Doctoral Committee:

Professor Nicholas Kotov, Chair
Professor John Kieffer
Professor Levi T. Thompson Jr
Assistant Professor Charles W. Monroe

To my parents, Hsiung-Chung and Su-Ching,

and my love, Melanie

Acknowledgement

I am heartily thankful to my advisor, Dr. Nicholas Kotov, whose encouragement, guidance, and support from the initial to the final level enabled me to develop an understanding on the interesting and challenging projects so that I learned how to be a great scholar, a great team leader, and a great teacher. In the past 6 years your patience and tolerance gave me full freedom to explore all kinds of interesting topics. Your great expertise and knowledge as well as your enthusiasm and passion for work will always enlighten my future life and career.

Next I would like to thank my committee members for their precious advice. I thank Prof. Kieffer and Prof. Thompson for letting me use their equipments to characterize my samples. Thank you to Prof. Monroe for his guidance on AC impedance measurement and simulation.

Thanks to all Kotov group members, Dr. Edward Jan, Dr. Ming Yang, Dr. Meghan Cuddihy, Dr. Daniel Lilly, Dr. Bongsup Shim, Dr. Ashish Agarwal, Dr. Sudhanshu Srivastava, Dr. Paul Podsiadlo, Dr. Y.X. Bai, Dr. Jun Li, Jian Zhu, Christine Andres, Huanan Zhang, and Joong Bahng, for your help and support over the years. A special thanks to Dr. Edward Jan. Your accompany, encouragement, and advice helped me overcome all the down times and stay positive in research and in life. I also offer my

regards and blessings to all of those who supported me in any respect during the completion of the project.

Thanks to my lovely fiancée, Melanie Hayes, for your endless love and support. I could not go through the crucial final stage of my PhD career without your encouragement and selfless care. Thanks to Brad and Tally Hayes for treating me as part of the family.

A special thank you to my best friend and my best-man-to-be Ian Chen. Thank you for being there for me since Day 1 of my life in Michigan. You cheered and backed me up in all the circumstances when I was frustrated and lost. And you were right! Lunch hours and Friday nights could not be any better without you.

I'm also deeply grateful to my friend Ching-Chin Pun for your selfless help and accompany. Thanks to my friends, Hsun-Yi, Jacob, Chien-Chou, and Chin-Yi, Robert, Tony, Emma, David, Edward, Sarah, Mitchell, James, Finn, Holly, Pei-Chen, and Wan-Hsiu for supporting me through difficulties and sharing joy and tears in this foreign country. Every footprint we have ever had together will never fade.

Finally, and most importantly, I would like to thank my parents Hsiung-Chung Ho and Su-Ching Chen, my sister Iris Ho, and brother-in-law Coen Blaauw. I could never get this far without your love and full support. Thank you Mom and Dad. I love you.

Table of Contents

List of Figures

List of Tables

Abstract

Layer-by-layer Assembly of Nanocomposites for Energy Applications

by

Szushen Ho

Chair: Nicholas Kotov

In the dissertation we utilized the versatility of layer-by-layer assembly to explore the possibilities of improving membrane characteristics in energy-related applications using such technique. Nanocomposite membranes comprising common polymers and state-of-art nanomaterials were fabricated by LBL technique. Physical and electrochemical properties, as well as performance in actual energy devices were intensively investigated. In fuel cell applications, Pt nanoparticle decorated carbon nanotubes and carbon nanofibers were manufactured into freestanding membranes for the use in fuel cell MEAs. SWNT and CF in LBL membranes formed extensive percolation networks and contributed to enhanced electronic and proton conductivities. Platinum nanoparticles deposited on the sidewalls of SWNT and CF incorporated with Nafion

significantly increased the number of catalysis sites and improved the accessibility to TPBs. Substantially improvement in performance and catalyst utilization was recorded.

Thick and uniform zeolite membranes were also created by LBL means. Zeolite-L modified electrodes showed signal enhancement in ferrocyanide redox reaction. By investigating the physiosorption and transport behavior at the electrodes, we proposed that although redox species couldn't diffuse freely in and out the channel due to size restriction, the adsorption of redox species inside the PDDA/zeolite-L membranes changed the concentration profile dramatically in the vicinity of the electrode surface. The active electron/hole conducting nature inside unidirectional channels in zeolite-L nanocrystals also contributed to the increase of active redox surface area.

Lastly, a new generation of ionic conducting nanocomposite membranes for lithium batteries was presented. Through layer-by-layer assembly of ionic conducting PEO and robust fibrous polymer Kevlar, the resulting membranes exhibited superior mechanical strength, high flexibility, and good conductivity. Mechanical strength and modulus of PEO-Kevlar ICMs are the key factors for lithium dendrite suppression, and were estimated to be orders higher than conventional polymer electrolytes. Special inhibition of re-crystallization in PEO phase by LBL technique indicates wider and higher working temperature window. Although the mechanical properties of the PEO-Kevlar membranes manufactured in this study did not reach the theoretical value for complete dendrite suppression, the results represent a step closer to next generation high capacity high power lithium batteries.

Chapter 1

Introduction

Fossil fuels are running out. For decades human have relied on fossil fuels to power the world and made daily life easier. However, according to BP Statistical Review of World Energy, the remaining world oil reserves are estimated to be 164.4 billion tonnes. About half the original energy stock has already been pumped out. Based on the production rate estimated in June 2008 at 80 million barrels (bbl) per day, deposits will only last for another 42 years. Extractable deposits of this fossil fuel will therefore disappear for good in 2050 (Source: BP Statistical Review of world Energy, 2007). It's extremely urgent to find alternative energy and also sustainable energy sources to help alleviate our dependence on soon-to-be-gone fossil fuels. Solar, wind, hydro, and geothermal are most sustainable energy sources as the energy that could be harvested from these sources is considered unlimited. However, these energy solutions require large-scale infrastructures and hardware to reach enough power density that may not be easily available. There is also no promising implementation of these sustainable energy solutions to modern mobile lifestyle yet. Automobiles and portable devices are for example two of the power-hungry industries where energy is the most demanded. They need smaller scale energy solutions that could provide sufficient support without

overwhelming size and added weight. Fuel cells, supercapacitors, and lithium batteries are better solutions that match the scale for these demands.

PEM fuel cells and direct methanol fuel cells are good candidates for auto industry because of their high energy densities. In fuel cells, membranes can be incorporated as the catalyst layer, the insulation layer to prevent fuel cross-over, or the membrane electrode assembly. To improve fuel cell performance, highly efficient membrane electrode assemblies (MEAs) are required. A well-designed electrode needs to possess both high electron and ionic conductivity in difference phases so the power of the fuel cells is not limited by internal transport bottleneck. Electrodes with well-controlled thickness and porosity to nanometer scale are also required so the balanced and well-distributed gas flow can be accommodated. A new means for MEA fabrication is also needed so the catalytic efficiency at triple phase boundaries (TPBs) can be optimized. TPBs are the sites where electrocatalysis and electrochemistry are taking place inside a fuel cell and where the energy stored in hydrogen is released. In short, active transport of electrons, protons, and gases to and from TPBs in fuel cells is the most crucial factor for high efficiency and performance.

For lithium batteries, increasing capacity represents the key bottleneck in many technologies exemplified by electrical vehicles, solar/wind energy conversion, flexible electronics, and health monitoring devices. Much attention had been paid to the optimization of both cathode and anode materials of lithium batteries. At the same time relatively little attention was given to cathode-anode separators, despite the fact that they

represent the crucial part of technological solutions for high capacity, high discharge rate, light weight, and safe electrical storage. Typically cathode-anode separators or lithium ion-conducting membranes (ICMs) are made from microporous polymer sheets impregnated with liquid or gel-like Li^+ electrolyte to provide high ionic conductivity. The major components of this type of ICMs are lithium hexafluorophosphate or lithium triflate dissolved in ethylene carbonate and dimethyl carbonate. Shortcomings of liquid ICMs setback their practical use including corrosion of the electrodes, limited temperature range of operation, leakage of electrolytes, and growth of metal dendrites during multiple charge-discharge cycles leading eventually to internal short circuiting of the batteries.

Importance of ICMs and their further development becomes particularly clear when considering the problem of dendrite growth. This process is responsible for many performance shortcomings and safety problems of traditional lithium ion batteries. Importantly, it is also the key roadblock for the development of batteries with lithium metal anode, which can approach the theoretical limit for lithium-based storage devices in respect to capacity, power, and weight. Prevention of dendrite growth for lithium anode will greatly improve battery performance compared to use of traditional lithium ion intercalation compounds but will require fundamental advances in ICMs. Different ways were proposed to prevent their formation, including mixing addictives to the electrolyte[1, 2], implementing polymer electrolytes with ceramic fillers[3-5], hybrid-gel electrolyte with fillers[6], and modification of growth morphology[7, 8], however this problem still persists. The mechanism of dendrite growth was intensively investigated

theoretically and experimentally[9-11]. The latest model proposed by Monroe and Newman suggests that although the formation and spread of dendrites during electrodeposition or battery charging/discharging cycles is inevitable under any polarization after a given time, sufficient compressive stress exerted on dendrite tips could dramatically inhibit their growth[12]. Dendrite formation can be prevented if the sheer modulus of ICM, G_{ICM}, can be two times higher than that for lithium, *i.e.* $G_{ICM} > 7$ GPa. This indicates that the resolution of dendrite formation lies in the development of lithium-ion conducting materials combining the high ion-conductivity and high mechanical properties. Potentially this can also address the problem with flammability of lithium batteries by eliminating flammable organic liquids from ICMs.

As a result, better membranes are required. Membrane technology is one of the key technologies that will be able to push energy industry forward. To recover clean and pure hydrogen without consuming too much power, we need membranes with robust construction, low thickness for high production rate, and high selectivity to improve recovery efficiency. To consume the energy stored in hydrogen in fuel cells, we also need the membranes to have high strength, high conductivity, and well-organized nanostructures to promote the efficiency of catalytic reactions. To promote ionic transport in lithium batteries, membrane research is the best place to start with. Despite the successes and advancements, many challenges, as mentioned earlier, still must be overcome before membrane technology becomes more widely adapted. New fashions to fabricate membranes with better structural control, greater mechanical and chemical

stability, greater reliability, improved fouling and corrosion resistance, or higher selectivity are required.

Nanoscale processing, or nanofabrication, represents the state-of-art material fabrication. It is the process of making functional structures with arbitrary patterns having minimum dimensions currently defined (more-or-less arbitrarily) to be ≤100 nm[13]. Many materials exhibit different physical or chemical properties when the dimensions approach nanoscale. For instance, quantum dots with diameter of several nanometers exhibit not only single-electron tunneling[14-17], uniform and mono-dispersed quantum dots with their one, two-dimensional assembly, and hybrid structures with proteins can also be easily engineered[18-23]. Carbon nanomaterials such as carbon nanotubes and carbon fibers also exhibit special properties like high electrical conductivity and mechanical strength when the dimensions approach in nanoscale[24-30]. By nanoscale material processing, one can preserve the extraordinary physical or chemical properties of nanomaterials and engineer new sensors, actuators, or even energy harvesting devices that was not possible by using bulk material processing. There are a couple of approaches in nanofabrication and can generally be divided into two main categories. The first category, called top-down process, includes conventional photolithography, electron-beam writing, and the "unconventional" molding[31, 32], embossing33, and printing[34, 35]. The second category, designated as bottom-up technique, includes all kinds of self-assembly of materials in nanoscale[36-40]. In these approaches, nanomaterials with different desired physical or chemical properties are used as basic building blocks to construct hybrid nanocomposites based on available inter-material interactions.

Layer-by-layer assembly (LBL) was first introduced in early 1990's[41]. It is one of the self-assembly means in bottom-up category and an advantageous thin film deposition technique. The assembly was systematically studied as a nano-processing tool in mid 1990's by Decher[42-44], Rubner[45-48], and Kotov[49-51]. Their pioneering work showed that layer-by-layer assembly is one of the most dynamic nanofabrication techniques available. First of all, layer-by-layer can be used in all kinds of nanocomposite construction, organic or inorganic, or mixture between the two. The versatility of layer-by-layer assembly makes it possible to incorporate nanoparticles[51-57], nanotubes[58-60], nanowires[52, 61], nanoplates[62-64], proteins[65, 66], and even virus[67] into thin film construction for functional materials. Second, layer-by-layer assembly, by comparison to other nano-processing methods such as photolithography and electron beam writing, is a very simple process. Each layer of material deposition generally involves only three straightforward steps: dipping of the substrate in nanomaterial dispersion, rinsing with deionized water, then blow dry. Because of the simplicity, the process can easily be automated and scaled up. Third, LBL assembly is robust by its reproducible material structures and qualities. And forth, layer-by-layer assembly has unique nanostructural controllability because the thickness of each layer can be fine-tuned within nanometer scale by varying deposition parameters. Through sequential deposition of oppositely charged polyelectrolytes onto the substrate to form a thin film, membranes can be finely tailored to desired properties at molecular level (Figure 1.1).

Although organic molecules provide an enormous structural diversity and tunability in terms of potential properties or processability, they also typically suffer from a lack of stability when exposed to heat, oxidizing agents, electromagnetic radiation, or dehydration. Layer-by-layer multicomposites, consisting of two or more different elements, make it possible to combine different desirable properties in one material. The main driving forces in LBL technique are electrostatic force, hydrogen bonding force, van der Waals force and hydrophobic force. Layer-by-layer assembly gives an improved molecular manipulation of the materials that make up the multicomposites. It also provides unprecedented uniform and dense loading of selected material within the matrix. The most important advantage of LBL assembly lies in the result of high-quality, well-ordered and substrate conforming structures. Membranes made by LBL assembly are highly homogeneous and defects free.

In this dissertation, we utilized the versatility of layer-by-layer assembly to explore the possibilities of improving membrane characteristics in energy-related applications. Nanocomposite membranes comprise common polymers and state-of-art nanomaterials were fabricated by LBL technique. Physical, mechanical, optical, and electrochemical properties, as well as performance in actual energy devices were intensively investigated.

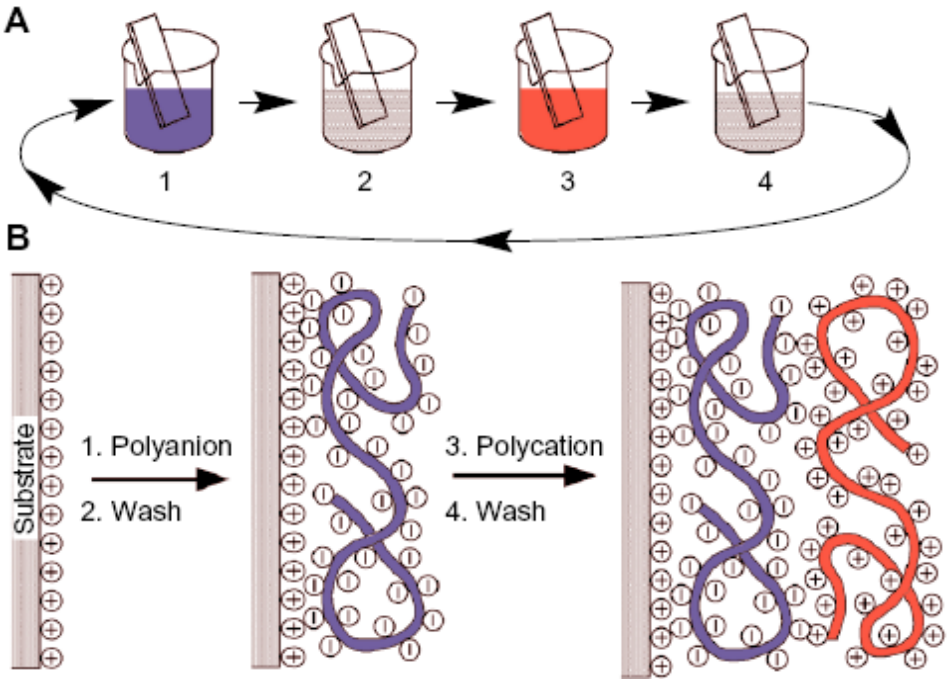

Figure 1.1 (A) Schematic of a LBL process[1] which includes substrate dipping steps in 1. polyanion, 2. rinsing water, 3. polycation, and 4. rinsing water. (B) Simplified expression of molecular formation of polyelectrolyte multilayers.

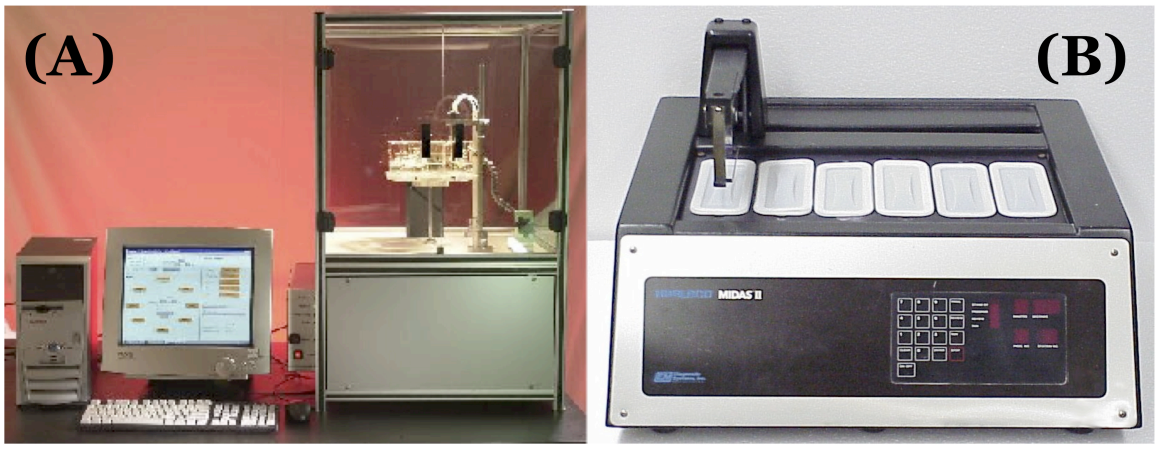

Figure 1.2 Fully automated robots for layer-by-layer assembly: (A) Nanostrata; (B) Slide stainer.

Chapter 2

Carbon LBL Membranes and their Applications

2.1 Layer-by-layer assembly of carbon materials

Carbon is one of the most abundant elements on earth, and the fourth most abundant element in the universe by mass after hydrogen, helium, and oxygen. There are several allotropes of carbon of which the best known are graphite, diamond, amorphous carbon, and carbon nanostructures (Figure 2.1). The physical properties of carbon vary widely with the allotropic form. Carbon nanocolloids such as carbon nanotubes (CNTs, single-walled and multi-walled) and carbon fibers (CFs) have shown exceptional high mechanical properties, electrical properties and chemical reactivity while having low density and high aspect ratio. They are potential candidates in energy related applications as they can be made into robust membranes easily by LBL assembly. CNTs, especially single-walled carbon nanotubes (SWNT), have many unique properties such as 1 TPa of Young's modulus ***(E)***, 30 GPa of tensile strength ***(T)***, and unusual electrical conductivities[68], which drive prompt efforts to exploit their properties by constructing a composite, grafting into a substrate, or dispersing into a solution. The origin of unusual properties of CNTs comes from the sp^2 hybridized C=C double bond which is known to be the strongest bond in nature and the nanosize tubular structure with a high aspect ratio which explains unique chemical and electrical properties of a single CNT. However, the

challenges of the CNT research mostly come from the difficulties in incorporating nanoparticles into a solution and a composite. Therefore, understanding and manipulation of these unique characteristics are important for building a desirable CNT system. In other words, morphological control of CNTs inside a polymer composite needs to be derived.

As reported by Pavoor *et al*, polymeric multilayers constructed by LBL assembly exhibited a dramatic improvement of mechanical properties and tribological lubrication properties compared to the pure polymers. However, polyelectrolyte is not the only option for LBL assembly; virtually any kinds of material can be assembled by LBL technique only if it has electrically active sites and can be dispersed in solution[69]. Therefore, sophisticated structural layered films with functional nanoparticles have been realized by LBL assembly, which can be applied for mechanical, magnetic, and optical functional materials[70]. Ostrander *et al*. have introduced different layered growth modes of nanoparticles depending on the states of exerting driving forces during LBL assemblies. The combination of electrostatic and van der Waals forces between nanoparticles-nanoparticles or nanoparticles-polyelectrolytes will play a role in shaping the nanoparticle deposition behavior such as normal growth or lateral growth[71]. Tang *et al*. reported that LBL assembled film of clay particles and polyelectrolytes has shown a natural bone like young's modulus and toughness with ionic crosslinking[72]. Mamedov et al. have reported that the SWNT-polyelectrolytes LBL film displays high mechanical properties because it includes amide bond linking between SWNT and polymer matrix and exceptionally high loading of SWNT with pseudo-homogeneity[70]. Another example

of SWNT – Polyelectrolyte LBL assembly has corroborated that the film has 2-dimensionally ordered and well dispersed morphological structures[73].

Hydrogen bonding interactions and van der Waals forces are also important driving mechanisms, which enable LBL assembly with a wide selection of non charged polymers, nanoparticles, and nanocolloids[48]. Although LBL assembly based on these weak forces interactions has only started to draw attention recently, they provide even more versatility and options for people to design nanocomposite materials, such as patterned nanoscale structures and porous membranes[74].

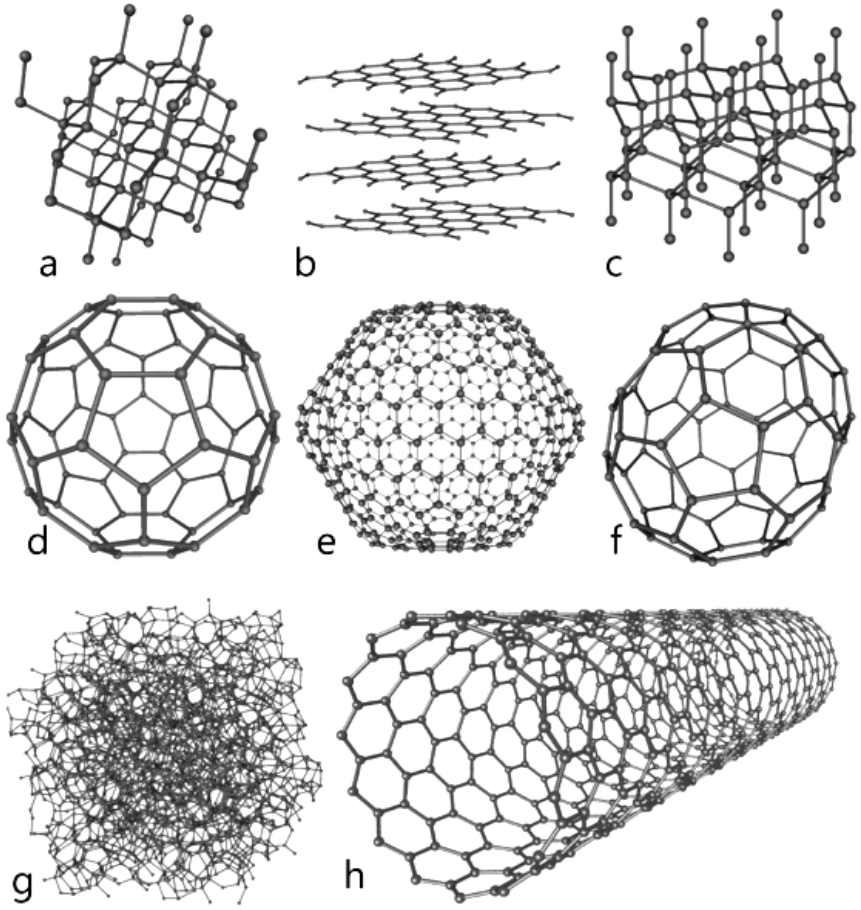

Figure 2.1 Carbon crystaline structures: diamond (a), graphite / carbon fiber (b), lonsdaleite (c), fullerene (bucky ball, d, e, and f), carbon nanotubes(h, SWNT , MWNT)

2.2 Mechanical Characterization of SWNT/CF LBL Membranes

Carbon nanotubes (CNT) and carbon fibers (CF) need to be dispersed in either polymers or surfactants in order to be incorporated in layer-by-layer assembly. Poly(styrene sulfonate) (PSS) is a very handy polymer for this purpose. Generally, 1 mg of SWNT or CF can be well dispersed in 1 wt% of PSS polymer solution with sufficient sonification. Through π-π stacking of PSS on SWNT / CF sidewalls, the dispersion of CNT or CF show absolutely no aggregation, and is extremely homogeneous. PDDA or PVA are commonly used as counter polyelectrolytes, which utilize electrostatic force and hydrogen-bonding as inter-layer bonding force respectively. Low cost, high availability, and strong affinity with PSS-wrapped SWNT/CF make PDDA and PVA the most popular polyelectrolytes to work with. AFM image of PVA-SWNT showed very well dispersed SWNT in PSS as well as very homogeneous deposition on the substrate (Figure 2.2(A)). Cross-section SEM image of a $[PVA\text{-}SWCNT]_{200}$ membrane shows the approximate thickness of 800 nm (Figure 2.2(B)). Each bilayer deposited has averaged thickness of 4 nm. These results suggest that with layer-by-layer assembly, one is able to control the thickness of membranes to nanometer scale.

Mechanical properties of carbon LBL membranes were tested using the tensile test setup (Figure 2.3). Specimens with dimension 1 mm by 25.4 mm were prepared and mounted on the machine. The specimen was pulled with increasing force. High sensitivity sensors were implemented to measure the force applied and the deformation of the specimen. Young's modulus of the specimen was obtained from the initial linear region of stress-strain relationship. The specimen was pulled continuously until they

broke, and that's when the ultimate strength of the specimen was obtained. Another way to get the Young's modulus of the LBL membranes is by bulging test. The difference between tensile test and bulging test is that, in tensile test, specimen undergoes one-dimensional stretching under tensile stress, while in bulging test, a uniform and distributed pressure is applied to an area of the membrane where the whole area undergoes deformation. By using bulging test one can obtained more averaged mechanical properties by stretching the membrane three-dimensionlly. Additionally, since pressure is the main driving force in most of the membrane applications, using bulging test gives more precise estimation on how a membrane perform in real life situations.

A homemade bulging system was design and setup to for this purpose (Figure 2.4). As-prepared LBL membranes were attached to the sample holder, and then mounted on the bulging test system where a pressure was applied to the sample by a pump. An optical interferometer was coupled with the bulging system to monitor the deformation of the membrane. Some optical interference patterns obtained from interferometer during a bulging session of a $[PVA\text{-}SWNT]_{150}$ membrane can be found in Figure 2.5. By counting the number of rings in each picture, one can relate the pressure applied to the deformation of the membrane. Each gap represents deformation of the membrane at half of light source's wavelength. Through linear fitting, one can get Young's modulus from bulging data (Figure 2.6). The results showed that the ultimate strength of carbon nanotube LBL membranes was in the range from 400 to 500 MPa, which is higher than that of brass (250 MPa) and cast iron (200 MPa), and is comparable to some types of stainless steel

(340 – 1900 MPa). The Young's modulus obtained from tensile and three-dimensional bulging test was 19-43 GPa, while in literature the value for stainless steel is 210 GPa. Characterization of mechanical properties suggested that carbon nanotube LBL membranes possess very high strength, so they can be utilized in applications where high stress or pressure is expected. At the same time, high elasticity of the membranes brings huge versatility and high degree of freedom to the design of experiments that one has more flexibility in implementing the membranes.

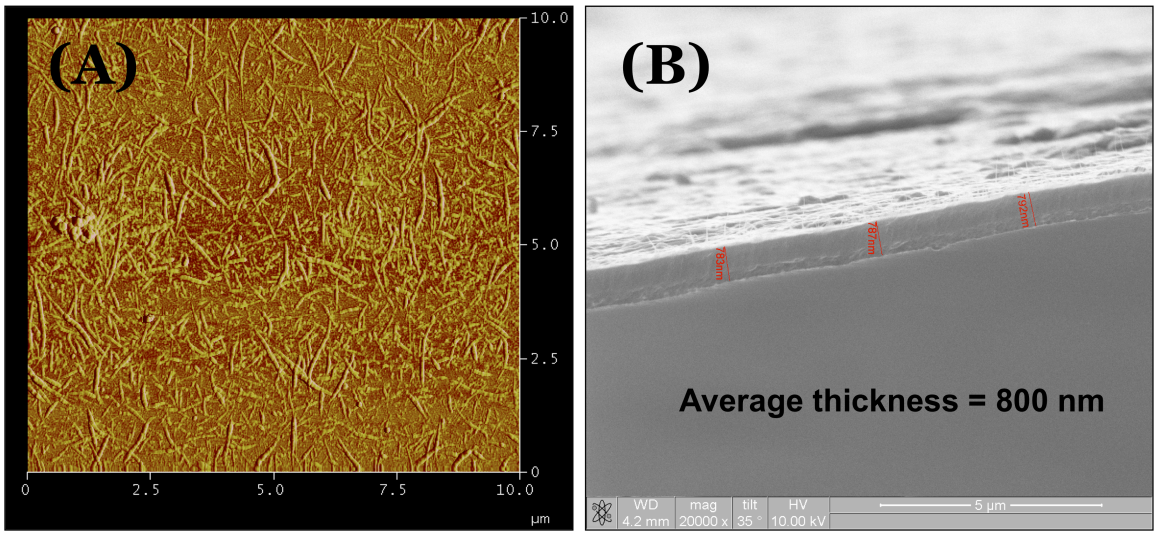

Figure 2.2 Layer-by-layer assembly of PVA and PSS-CNT. (A) AFM image of PVA/single-walled CNT on silicon wafer. (B) SEM image of $[PVA\text{-}SWCNT]_{200}$ with cross-section view.

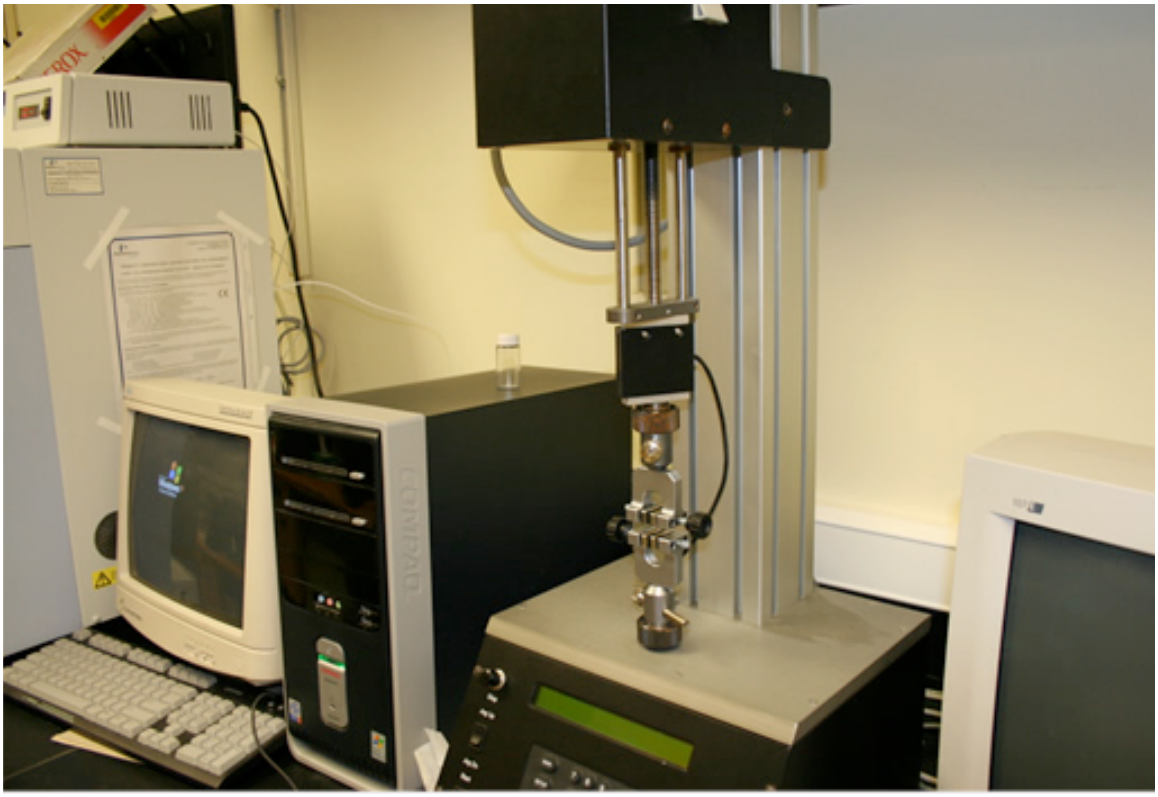

Figure 2.3 Tensile test machine for mechanical properties.

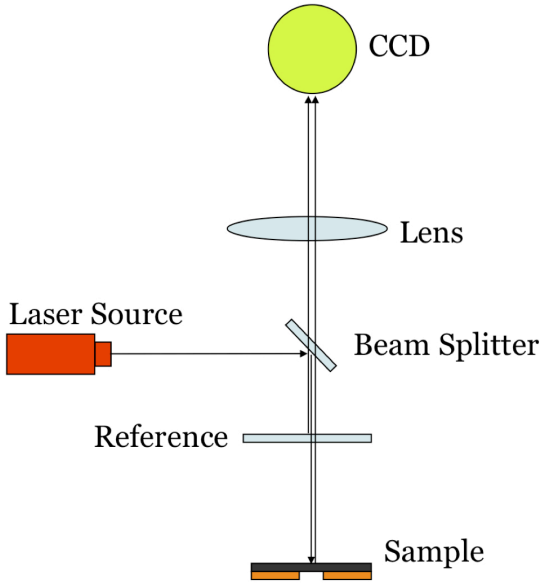

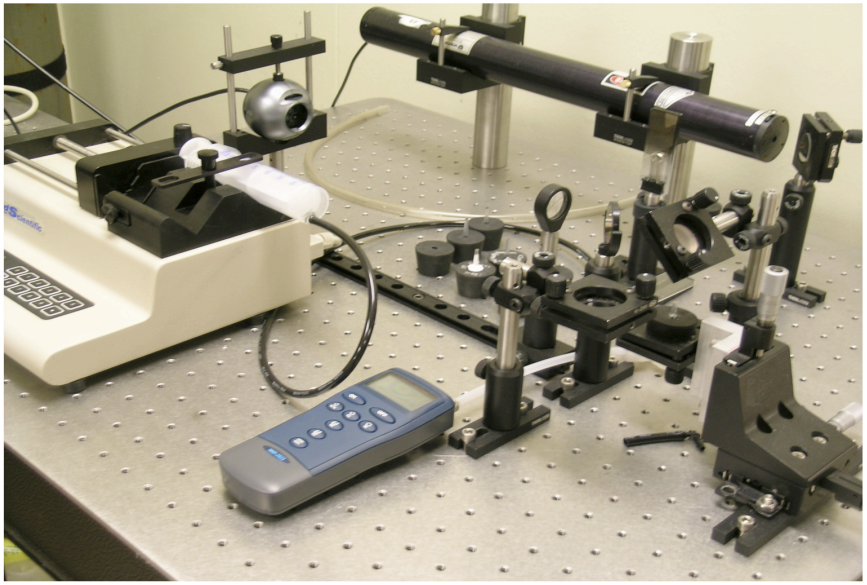

Figure 2.4 Bulging system coupled with optical Interferometry. A pressure is applied to the sample, monitored by high sensitivity pressure gauge, while optical interferometer monitors the deformation of the sample membrane.

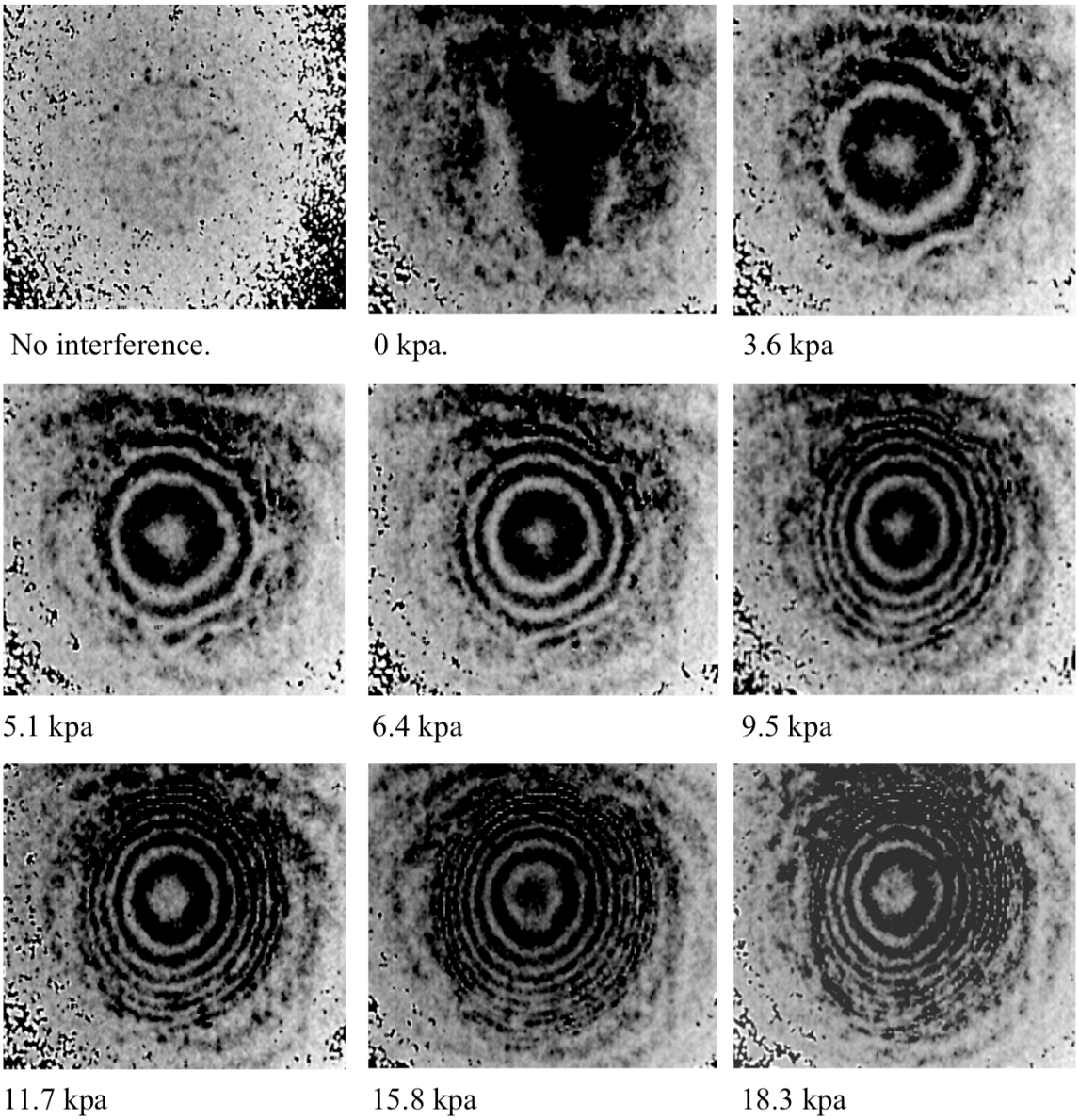

Figure 2.5 Optical interference patterns obtained from interferometer during a bulging session. By counting the number of rings in each picture, one can relate the pressure applied to the deformation of the membrane. Through linear fitting, one can get Young's modulus from bulging data.

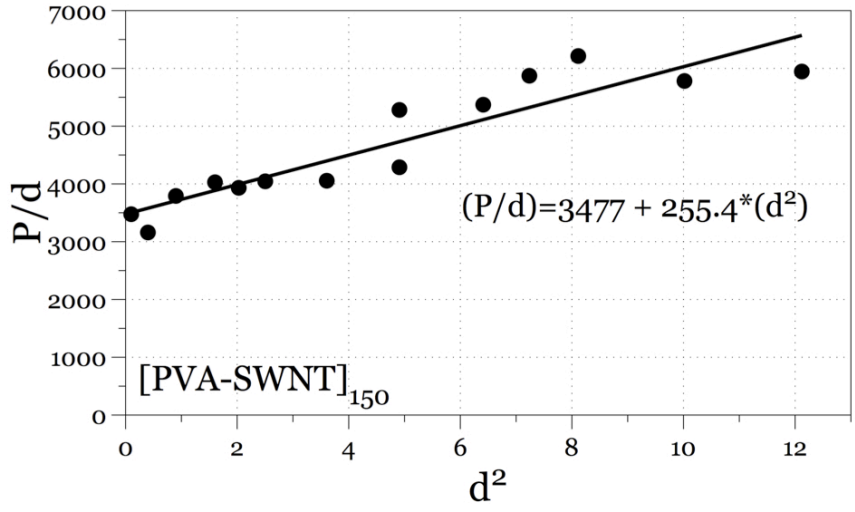

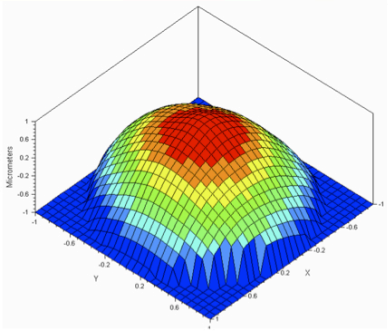

$$\left(\frac{P}{d}\right) = f(d^2) = A(d^2) + B$$

$$A = C_1 \frac{E}{1-\nu} \frac{t}{a^4}$$

$$B = C_0 \frac{E}{1-\nu^2} \frac{t^3}{a^4} + C_2 \frac{\sigma_0 t}{a^2}$$

Figure 2.6 Linear fitting of bulging data from a $[PVA\text{-}SWNT]_{150}$ membrane.

	Tensile Strength (MPa)
LBL SWNT membrane	**450±50**
Steel	340-1900
Brass	250
Cast Iron	200

	Young's Modulus E
LBL SWNT membrane	19-43 GPa
Steel	210 GPa

Table 2.1 Tensile strength and Young's modulus of CNT LBL membranes.

2.3 Carbon Nanotube LBL Membranes for Gas Separation

Ethane/Ethylene separation has long been a challenge because of their similarity in size, mass, geometry, and interaction parameters. Carbon nanotubes and related nanostructures are proven to have good selectivity between the two species. Simulation results published by Cruz and co-workers showed a threshold (crossover) pressure, in the lower vicinity of 10 bars (1 MPa), below which ethane molecules are preferentially adsorbed over ethylene. Selectivity is not large, typically below $S = 4$. This preferential ethane adsorption is attributed to the larger dispersive forces that characterize the ethane molecules, and verified by the calculation of the corresponding isosteric heats of adsorption and low coverage Henry's constants[75]. In this project we proposed using carbon nanotube LBL membranes as ethane/ethylene separation membranes. High loading of carbon nanotubes in the membranes could contribute to high physiosorption of ethane molecules on carbon nanotubes and lead to high selectivity over ethylene. High strength of CNT LBL membranes would ensure the integrity of the membranes under high pressure, and the small thickness could also contribute to high permeation flux.

A homemade gas separation system is demonstrated in Figure 2.7(A). LBL membranes to be tested are sandwiched in between two stainless steel meshes and housed inside the test cell. Pressure transducers are setup to constant monitoring and recording pressure inside the system. For the times smaller than t=0, the whole system is evacuated so that no penetrant molecules remain in the membrane. Starting at t=0 with an upstream pressure P1, and vacuum on the downstream side, the total amount permeated through the membrane in time form a non-linear increase in the transient state into a linear increase in

the steady state when an equilibrium concentration profile in the membrane is reached (Figure 2.7(B)). We can get the diffusion coefficient D by:

$$D = \frac{L^2}{6\theta} \quad (\frac{m^2}{s}) \qquad \text{(Eq. 2-1)}$$

where L is the thickness of the gas separation membrane, and θ is the lag-time defined in Figure 2.7(B). Then, the permeability P is:

$$P = \frac{\Delta p_2}{\Delta t} \frac{1}{(p_1 - p_2)} \frac{V_c}{RT} \frac{L}{A} \times 22400 \quad \text{(barrer)} \qquad \text{(Eq. 2-2)}$$

For the separation of hydrogen, ethane, and ethylene (Figure 2.8), $[PVA\text{-}SWNT]_{400}$ membrane was mounted in the permeation cell with an circular opening of 500 μm in diameter as active gas separation area. 415 torr of pressure was used as driving force. One can calculate the diffusion coefficient of H_2, C_2H_6, and C_2H_4 through the CNT LBL membrane as well as permeability of individual species (Table 2.2). The results showed that the permeability of the three has the ratio of 3.5:1:1.1. Hydrogen has highest permeability of all three as expected because of it's small in size, but the selectivity of ethylene over ethane is not as good as in the literature. Possible reasons include:

1. Gas molecules did not actually go inside carbon nanotubes. In the literature, the simulation was based on the gases flowing inside carbon nanotubes instead of going through porous CNT LBL network. Preferential adsorption of ethane on carbon nanotubes was then not as significant.

2. Driving pressure was too low compared to the literature. In the literature, 10 bars of pressure (7500 torr) was used in the literature to obtain selectivity of 4. In our experiments, only 415 torr of pressure was applied to the separation membrane, and low

driving pressure very likely retarded selectivity. There was virtually no way to crank up the pressure to near 10 bars without breaking the membranes as the thickness was only around 1.5 μm.

3. Perhaps there was no preferential adsorption of ethane molecules on CNTs in our LBL membrane. The separation was solely based on size separation, so the selectivity suffered.

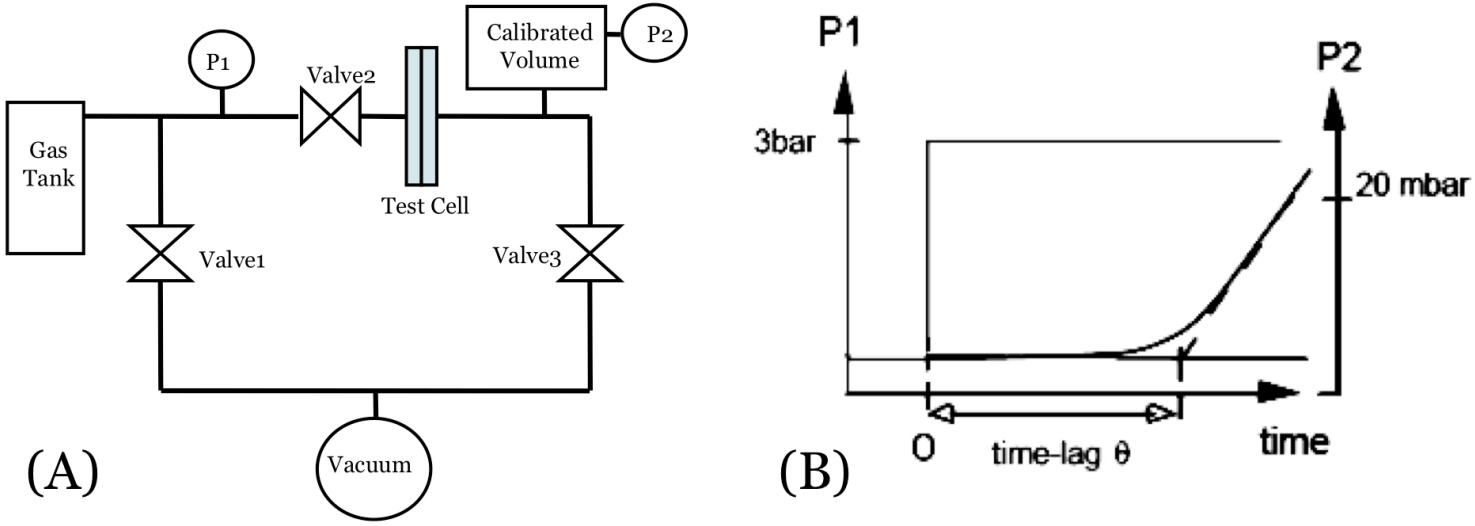

Figure 2.7 (A) Illustration of gas separation setup. CNT LBL membranes were sandwiched in between two stainless steel meshes and housed inside the test cell. Pressure transducers were setup to constant monitoring and recording pressure inside the system during gas permeation tests; (B) From pressure p_1, p_2 and lag-time θ, one can easily calculate diffusion coefficient D and permeability P.

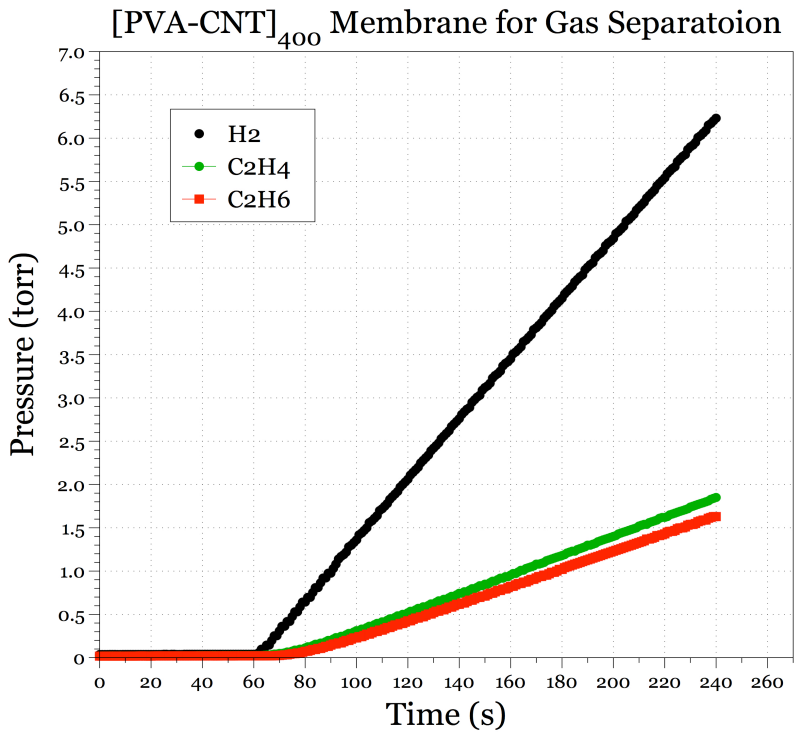

Figure 2.8 Separatino of hydrogen/ethane/ethylene using $[PVA\text{-}CNT]_{400}$ LBL membrane. The permselectivity was calculated to be 3.5:1.1:1.

Gases	Θ (s)	D*e14 (m^2/s)	Permeability P (barrer)
Hydrogen	2.806	5.94	0.0128
Ethylene	13.534	1.23	0.0037
Ethane	18.365	0.908	0.0034

Table 2.2 Lag time, diffusion coefficient, and permeability of hydrogen, ethane, and ethylene through $[PVA\text{-}SWNT]_{400}$ membrane at room temperature.

Since the CNT LBL membranes had been shown to perform better based on size selectivity, hydrogen/nitrogen separation was tested with $[PVA\text{-}SWNT]_{400}$. In the hydrogen recovery industry, the best way to do it is to pass the feedstock through stainless steel membranes with doped Pd metal at 500 °C. The selectivity of hydrogen over nitrogen could range from 150 to 600, depends on the ratio of hydrogen and nitrogen in the upstream. However, with this method a lot of energy is required to generate the heat required to activate all the sites on stainless steel membranes. At room temperature, the selectivity of Pd-stainless steel membrane becomes only 3.7. With $[PVA\text{-}SWNT]_{400}$ membranes, the selectivity of hydrogen over nitrogen was determined to be 2.7 (Figure 2.9). The performance is very similar to polypropylene membrane of 3.5, but compared to polyimine/Polyethersolfon membrane of 56, cellulose acetate of 33, and polyimide of 35.4, CNT LBL membranes are currently not yet good candidates for hydrogen regeneration applications. However, there are still possibilities through surface modification of carbon nanotubes to introduce active recovery sites. This should be a very interesting topic for future research and development.

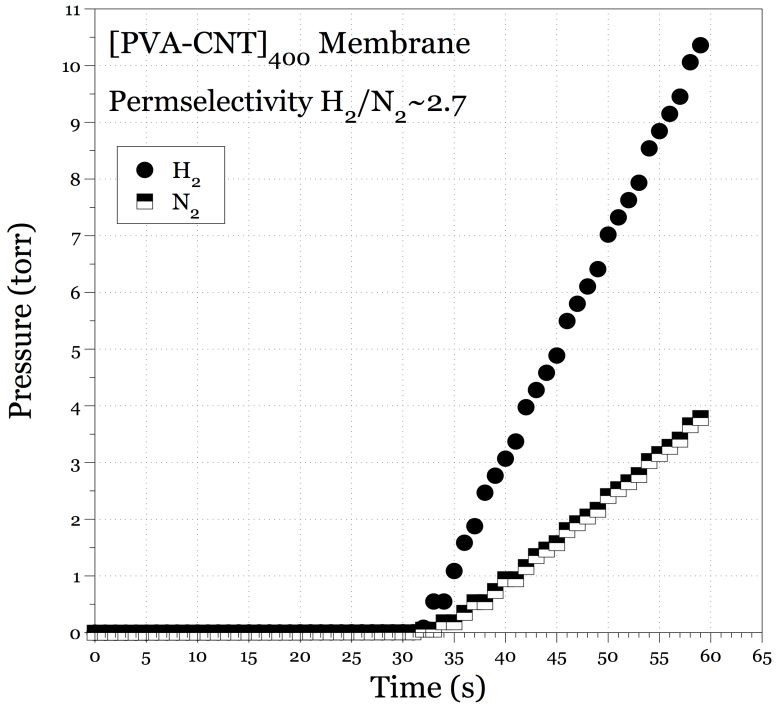

Figure 2.9 Separation of hydrogen/nitrogen using $[PVA\text{-}CNT]_{400}$ LBL membrane. The permselectivity was calculated to be 2.7.

2.4 SWNT/CF LBL Membranes for Fuel Cells

2.4.1 Introduction

Recently layer-by-layer assembly method has been used to prepare membranes for PEM fuel cells and direct methanol fuel cells because of its special and advantageous characteristics. These membranes are incorporated into fuel cells stacks as the catalyst layer[76], the insulation layer to prevent fuel cross-over[77, 78], and the membrane electrode assembly[79, 80]. LBL technique has outstanding capability to blend different conflicting requirements into ultra-thin membranes. It is possible to deposit conformal coatings on any surface of complex geometry while controlling the thickness and porosity to nanometer scale. It is also possible to design and fabricate membranes with high electrical and ionic conductivities at the same time. Generally a membrane electrode assembly (MEA) consists of cathode, anode, and proton exchange membrane. The three parts are equally important as they together hold the key to high performance and durability. Inside cathode and anode one can find high loading of metal catalysts, commonly platinum, in micro or nanoparticle forms, mixed with carbon black and proton conducting Nafion, to create so called triple-phase boundaries (TPBs). TPBs are the sites where electrocatalysis and electrochemistry are taking place inside a fuel cell and where the energy stored in hydrogen is released. Active transport of electrons and protons to and from TPBs is very crucial for high efficiency and performance. Layer-by-layer assembly has advantages in the field of fuel cell because nanomaterials deposited by the technique are very uniform and well distributed. Carbon LBL membranes also possess high strength

and durability that could hold against degradation in harsh acidic environment inside fuel cells.

Farhat and Hammond used layer-by-layer assembly to make ionic and electronic conducting polymer multilayer film as catalytic electrodes[80]. Films of polyaniline (PANi)/poly(acrylic acid) (PAA) or PANi/poly(acrylic acid)-co-polyacrylamide (PAA-co-PAAm) of 3.0 μm thickness were pH-tuned to induce porosity as they were assembled. Reductive precipitation of platinum salts yielded good metal loading with maximum Pt loading of 0.3 mg/cm^2 shown to have relatively high and stable electrical conductivity of 2.3 S/cm, and an ion conductivity of up to 10^{-5} S/cm. The same group also utilized layer-by-layer assembled membranes as the proton exchange membrane in fuel cells[77]. The composite membranes are constructed through the layered assembly of ionically conductive polymer multilayer thin films on top of a porous polycarbonate membrane. Under ambient condition, the fuel cell using poly(ethylene oxide)/poly(acrylic acid) (PEO/PAA) composite membrane can deliver a maximum power density of 16.5 mW/cm^2 at a relative humidity of 55%.

Ligand-stabilized platinum nanoparticles was used to build three-dimensional nanostructured electrodes using layer-by-layer assembly by Kostelansky et al[81]. After only 5 layers of deposition, the Pt loading could reach 5.6 μg/cm^2, with current density as high as 0.11 A/mg-Pt at 0.9 V. Farhat and Hammond later utilized layer-by-layer technology again to fabricate flexible ultrathin membrane electrode assembly for fuel cells. Different from their previous work, the new thin-film electrode did not utilize

conducting polymer or traditional metal or chemical deposition methods. Instead, LBL carbon-polymer electrodes were made from polyelectrolytes and stable carbon colloidal dispersions[79]. Weak polyelectrolytes linear poly(ethylene imine) (LPEI) and poly(acrylic acid) (PAA), strong polyelectrolytes poly(diallyldimethylammonium chloride) (PDDA) and poly(2-acrylamino-2-methyl-1-prepane sulfonic acid) (PAMPS) are used in the research. To insure acceptable electrical conductivity and good catalyst loading, both polyanionic and polycationic polymer solutions were pre-loaded with carbon colloids and platinum. LBL assembled films of weak polycationic LPEI(10mM, 100mL)/1μ-carbon(0.2g)/Pt(0.02g) with weak polyanionic PAA(10mM,100mL)/1μ-carbon(0.2g)/Pt(0.02g) or strong polycationic PDDA(10mM, 100mL)/HiSpec-3000(0.1g) with strong polyanionic PAMPS(10mM, 100mL)/HiSpec-3000(0.1g) are deposited on the substrate. These electrodes showed exceptional chemical stability under strong acidic, basic, and oxidizing media. The electrical conductivity is as high as 4 S/cm with ionic conductivity at the range of 10^{-3}-10^{-4} S/cm. Tested in galvanic cell, the best performed membrane delivered 3.0mW/cm^2.

In this project we used carbon nanotube and carbon nanofiber for ultrastrong LBL fuel cell MEAs for improved performance and durability. Single-walled carbon nanotube (SWNT) and carbon fiber (CF) loading in LBL membranes can be as high as 50% without phase segregation of dissimilar materials. Uniform distribution of nanotubes and nanometer control of the film structure through layer-by-layer assembly could contribute to an extensive percolation network where improved electronic and proton conductivities could be found due to a significant reduction of the tunneling energy required for inter-

particle charge-hopping step. Platinum nanoparticles deposited on the sidewalls of SWNT and CF with the incorporation of Nafion could significantly increase the number of catalysis sites and improve the accessibility to tri-phase boundaries (TPBs).

2.4.2 Deposition of Nanocatalysts on SWNT and CF

Platinum and platinum nanoparticles are the most general catalysts in MEA in fuel cells. To optimize utilization of Pt catalyst, Pt nanoparticles should form the triple phase boundaries and be in contact with the membrane electrolyte, carbon, and the reactant gases. Various deposition techniques have been investigated such as electrodeposition[82-84], sputtering deposition[85, 86], plasma sputtering[87, 88], chemical deposition of Pt nanoparticles on chemically modified polymeric composites[89], and self-assembly of Pt nanoparticles[76]. Wang et al utilized selective heterogeneous nucleation to grow size-controlled Pt nanoparticles on carbon nanotubes in solution[90]. The reduction of metal ion $PtCl_6^{-2}$ in ethylene glycol (EG), by the addition of sodium dodecyl sulfate (SDS) salt, resulted in high dispersions and high loadings of platinum nanoparticles on SWNT sidewalls without aggregation. The size of Pt nanoparticles can be controlled between 2.3-9.6 nm by reaction temperature, reducing agent, and metal ion concentration. Loading as high as 50% can be achieved by this method.

Following the synthesis protocol published by Wang *et al* with further optimization, we were able to obtain Pt nanoparticles with uniform size distribution with diameter around 1.5-3 nm. Figure 2.10 (A)-(D) are the TEM images of Pt-nanoparticle-decorated single-walled carbon nanotubes (A, B) and carbon fiber (C, D). Highly uniform nanoparticles were deposited along carbon nanotube bundles and covered nearly the whole sidewalls of carbon fibers. High resolution TEM images in (B) and (D) confirmed that the Pt nanoparticles are single-crystalline. Thermal gravimetric analysis (TGA) showed very steady patterns that, before reaching 400 °C moisture and amorphous carbon

were evaporated and burned, and from around 400 – 500 °C carbon fibers were burned, leaving platinum and some platinum oxide (Figure 2.11). The loading of Pt nanoparticles on carbon fiber in the three batches we synthesized was then determined to be as high as 35.24% (Table 2.3).

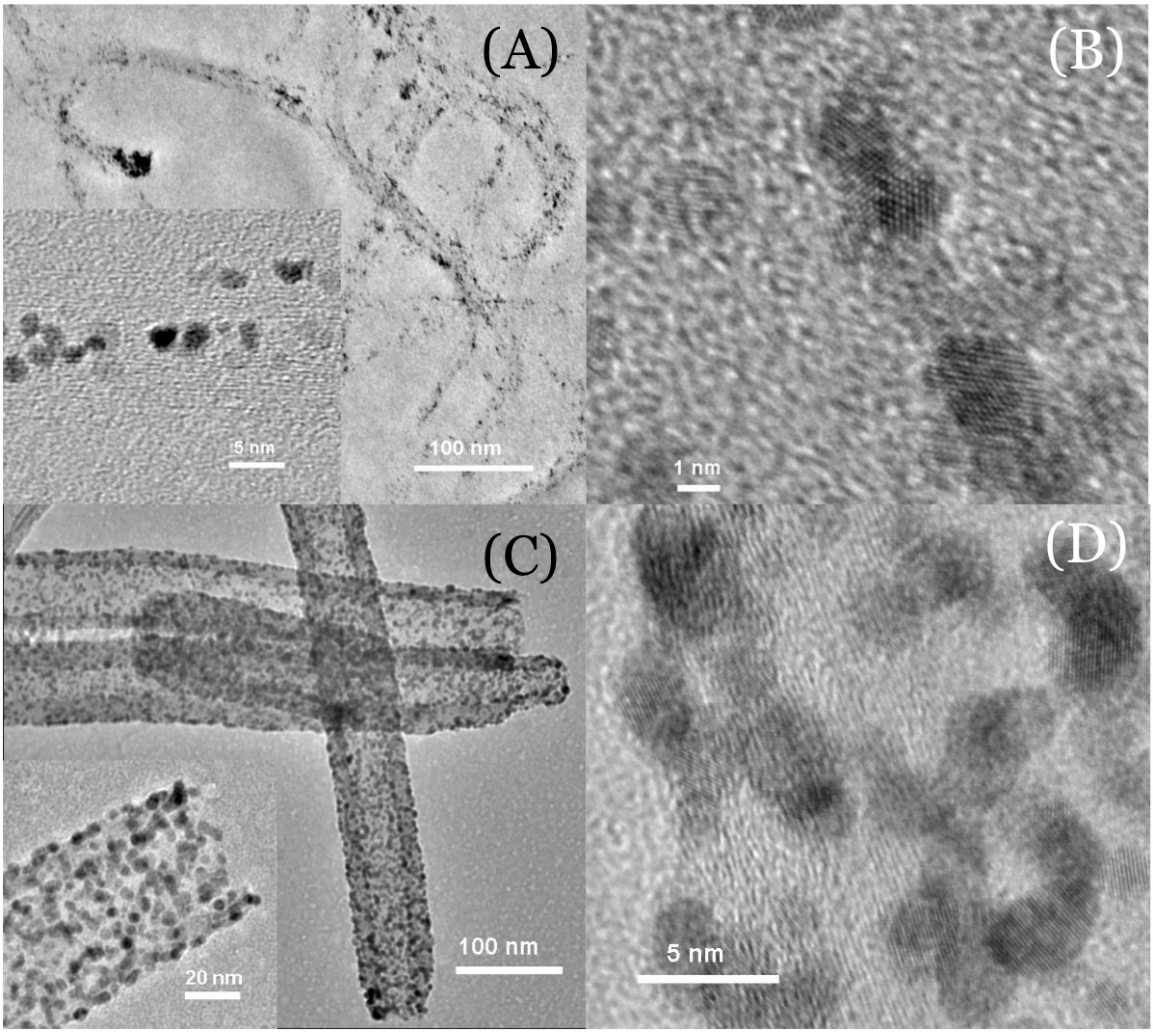

Figure 2.10 Pt nanoparticles deposited on CNT (A, B) and CF (C, D) using selective heterogeneous nucleation method. With improved synthesis recipe, we could deposit size-uniform Pt nanoparticles on the sidewalls with averaged diameter from 1.5 to 3 nm.

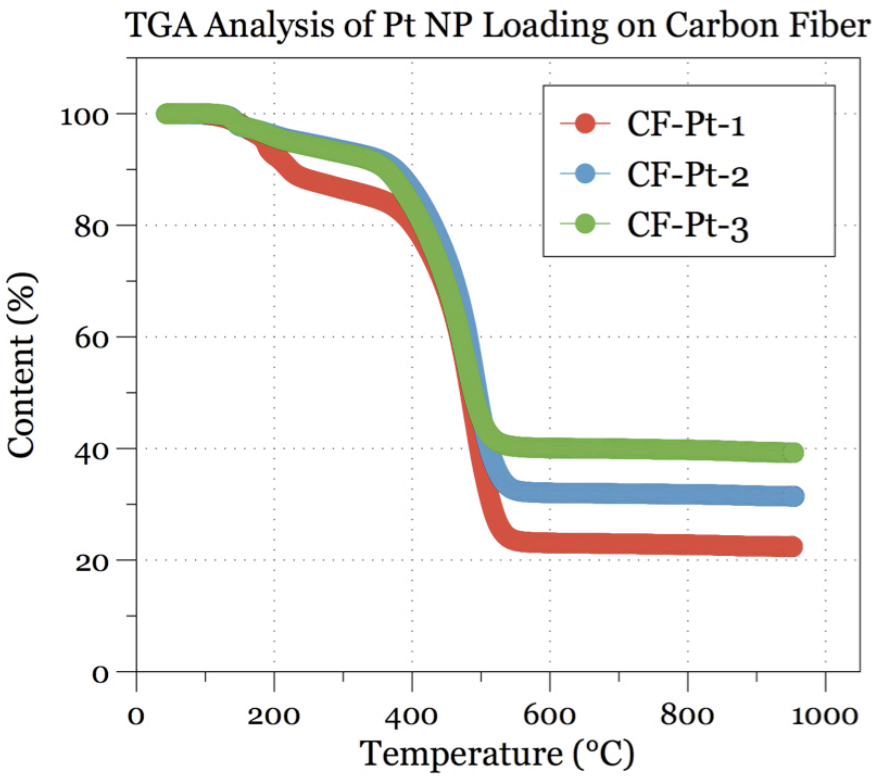

Figure 2.11 Thermal gravimetric analysis of Pt nanoparticle loading on carbon fibers from different batches.

Batch	Pt Loading (%)
1	18.28-19.50
2	26.37-28.10
3	33.03-35.24

Table 2.3 Pt nanoparticle loading on carbon fibers from different batches. Not the loading take into account the weight of residual iron catalyst used during carbon fiber manufacturing process.

2.4.3 LBL SWNT-Pt and CF-Pt Membranes for Fuel Cell MEAs

Layer-by-layer assembly of SWNT-Pt and CF-Pt was carried out by first dispersing SWNT-Pt and CF-Pt in 0.2 wt% Nafion-ethanol-water solution. 1 mg of SWNT-Pt or CF-Pt was dispersed in 1 ml of solution with at least 24 hours of continuous sonication. Both SWNT-Pt and CF-Pt dispersions showed no aggregation indicating good wrapping of Nafion polymer around SWNT-Pt and CF-Pt. Here Nafion not only played the role as a dispersing agent, but also created "on-site" triple phase boundaries at SWNT-Pt-Nafion and CF-Pt-Nafion interfaces. This is very crucial because now, on anode side, when hydrogen comes in to be in contact with platinum nanocatalysts, protons could be conducted through Nafion phase to proton-exchange membrane while electrons could go through carbon nanotubes or carbon fibers to be conducted to current collector and then the outer circuits. Same on the cathode side that protons could follow the passages created by Nafion on SWNT-Pt or CF-Pt to catalytic sites to react with electrons and oxygen.

Polyrthyleneimine (PEI) was used as counter polyelectrolyte to work with SWNT-Pt-Nafion and CF-Pt-Nafion as PEI and Nafion have very high affinity with each other. AFM image of one [PEI/(Pt/SWNT+Nafion)] layer on silicon wafer showed that high amount of SWNT-Pt on the surface (Figure 2.12). One can also see Pt nanocatalysts along SWNT bundles and also on the surface. SEM images of $[PEI/(Pt/CF+Nafion)]_{400}$ and $[PEI/(Pt/SWNT+Nafion)]_{400}$ showed very uniform membrane thickness from the cross-section (Figure 2.13(A) and (C)) and very dense and high loading of CF and SWNT from top view (Figure 2.13(B) and (D)). Dense deposition of CF or SWNT in the

membrane has an advantage that gas coming into the electrode can be better distributed to catalytic sites. Normally gas-diffusion layers made of carbon cloth are implemented to improve gas passage into the electrodes. Here, with dense, forest-like CFs and SWNTs we believe when hydrogen and oxygen come into the electrodes, the gas distribution would be better than traditional electrodes made with carbon black.

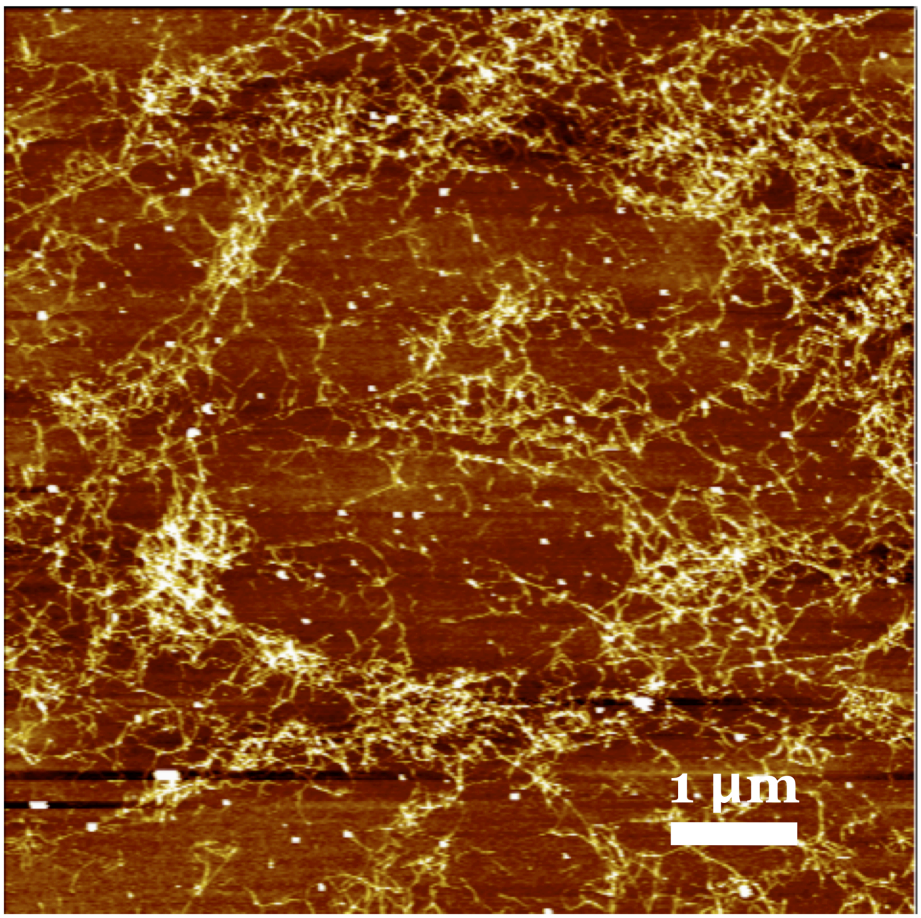

Figure 2.12 AFM image of Pt nanoparticle coated carbon nanotubes on silicon wafer. One layer of deposition. High amount of CNT-Pt was deposited on the surface. Pt nanoparticles are also visible along the sidewall of CNTs.

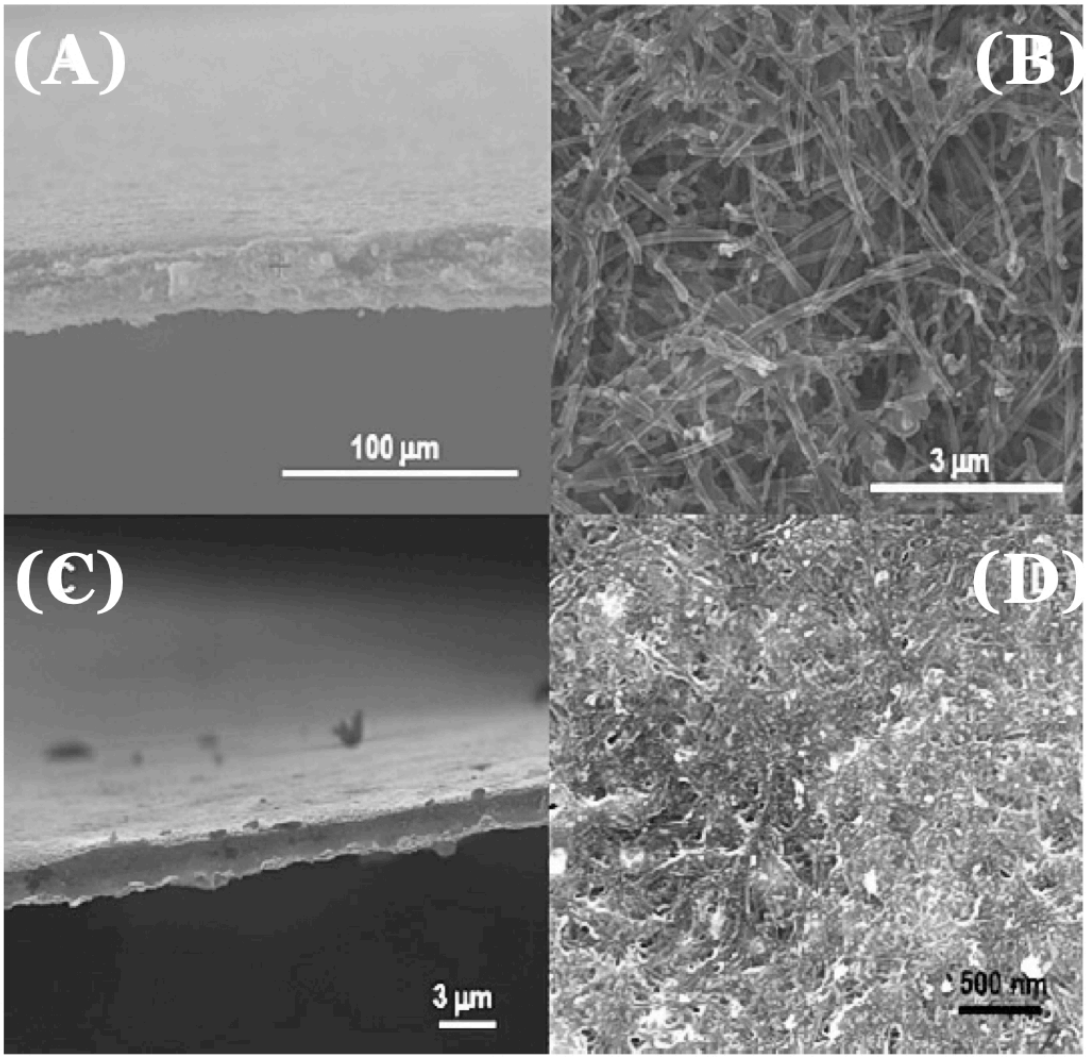

Figure 2.13 SEM images of $[PEI/(Pt/CF+Nafion)]_{400}$ (A,B) and $[PEI/(Pt/SWNT+Nafion)]_{400}$ (C,D)

2.4.4 Characterization of SWNT-Pt and CF-Pt LBL Electrodes

X-ray photoelectron spectroscopy (XPS) was first used to investigate oxidation states of the Pt nanoparticles deposited on carbon nanotubes and carbon fibers (Figure 2.14). In both SWNT-Pt and CF-Pt cases, the binding energy of 71.2 eV and 74.5 eV are corresponding to $4f_{7/2}$ and $4f_{5/2}$ orbital of platinum, indicating fully reduction of platinum precursor to Pt metal state. Polarization and power density curves were then obtained by mounting the LBL films as anodes in fuel cells (Figure 2.15). The fuel cell temperature was set at 80°C, H_2 and O_2 flows on fuel cell saturators are set at 100 sccm flow rates, with 100% relative humidity, and 90°C temperature. Polarization and power density results are listed in Table 2.4. The Pt loading in $[PEI/(Pt/SWNT+Nafion)]_{400}$ and $[PEI/(Pt/CF+Nafion)]_{400}$ was determined to be 0.26 and 0.2 mg/cm^2, with power density at 195 and 227 mW/cm^2. One can find the Pt utilization of Pt on CF is 1135 mW/mg while in SWNT case 750 mW/mg was obtained[91]. High catalyst utilization in carbon fiber electrode possibly came from:

1. Better gas diffusion inside carbon fiber electrode. From SEM images one can find that carbon fiber LBL membranes have higher porosity than carbon nanotube ones because of the size difference between SWNT and CF. The better the gas distribution is, the higher chance hydrogen reaches catalytic sites for reaction.

2. Carbon fibers are also longer than single-walled carbon nanotubes that they have higher chance to form better inter-connecting network for better electron and proton conduction.

3. Pt nanocatalysts on carbon fibers are more accessible than the ones on carbon nanotubes due to Nafion wrapping step. Nafion is more likely to block Pt sites on SWNTs because of the size of SWNTs.

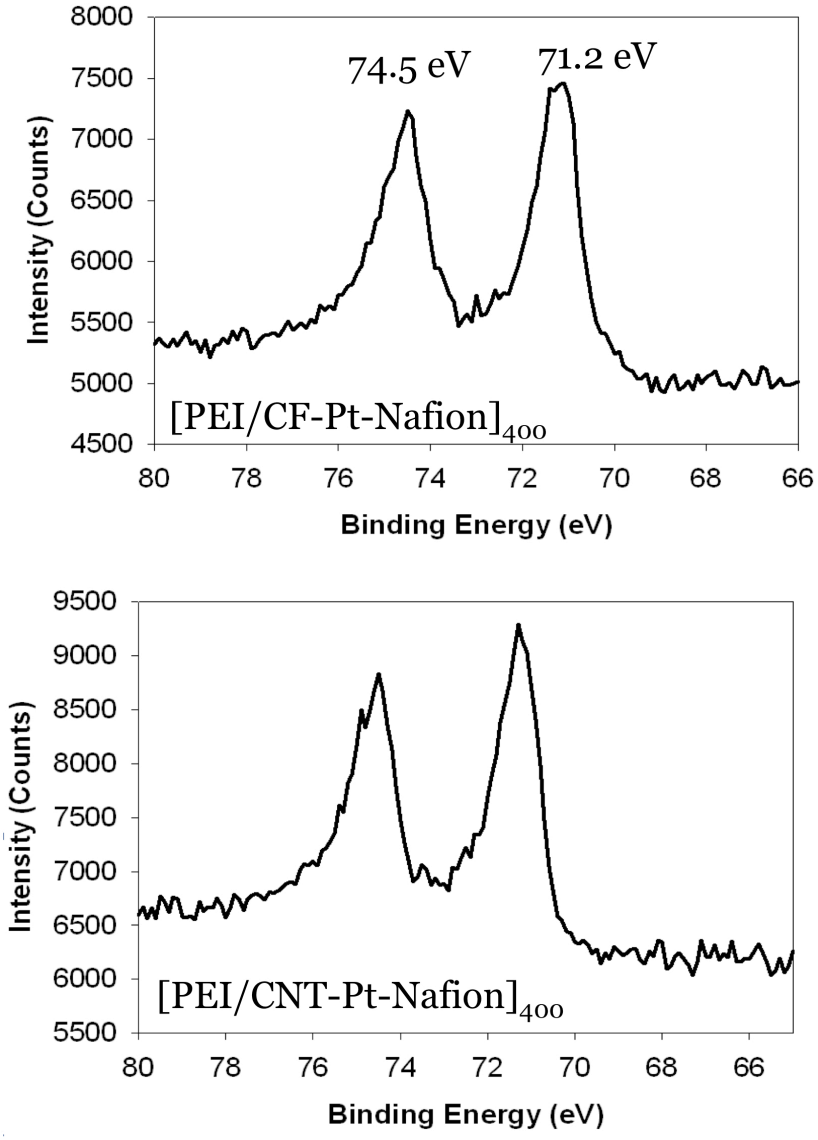

Figure 2.14 XPS spectra of CF-Pt and CNT-Pt LBL membranes confim the Pt on the sidewalls of CF and CNT were fully reduced to "0" state.

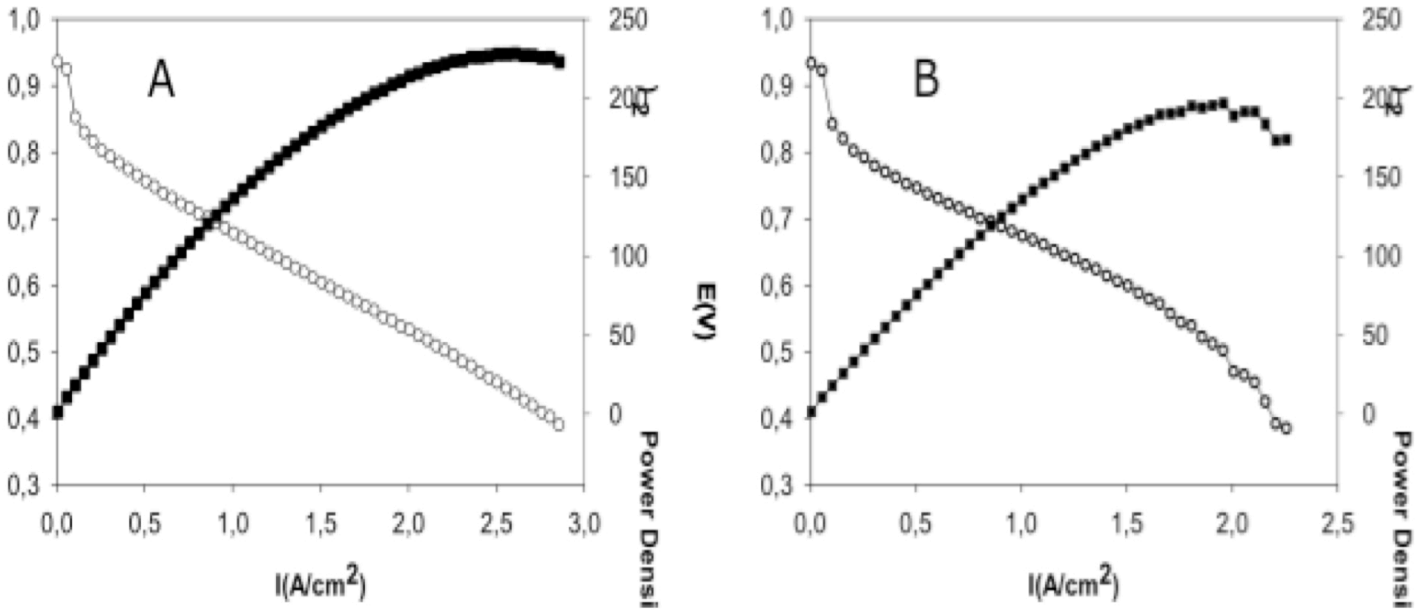

Figure 2.15 Polarization (○) and power density (■) curves of fuel cells with LBL film anodes : (A) [PEI/(CF-Pt-Nafion)]400 and (B) [PEI/(SWNT-Pt-Nafion]400 . Fuel cell temp: 80°C. H2 and O2 flows on fuel cell saturators are set at 100 sccm flow rates, 100% relative humidity, and 90°C temperature.

Group	System	Pt support	Anode loading (mg/cm²)	Cathode Loading (mg/cm²)	Peak Power Density (mW/cm²)	Pt utilization mW/mg
UM	$[PEI/CNT\text{-}Pt\text{-}Nafion]_{400}$	SWNTs	0.26	0.4870	195	750
UM	$[PEI/CF\text{-}Pt\text{-}Nafion]_{400}$	CFs	0.2	0.567	227	1135
MIT	LPEI/PSSM	Carbon black (CB)	0.5	0.5	0.2	0.32
MIT	LPEI/PSS	CB	0.5	0.5	2.7	5.40
MIT	LPEI/PAMPS	CB	0.5	0.5	3.6	7.20
MIT	POE/PMAA	CB	0.5	0.5	2.5	5
MIT	LPEI/PAA	CB	0.5	0.5	5.5	11
MIT	PDAC/PAMPS	CB	0.5	0.5	11.6	23.20
MIT	PDME/PAMPS	CB	0.5	0.5	6	12
MIT	POE/PAA	CB	0.5	0.5	16.6	33.20

Table 2.4 Comparison of PEM fuel cell MEAs manufactured using layer-by-layer assembly from different groups. Note the high peak power density and Pt utilization from CF-Pt MEA are the best performance among all.

2.5 Conclusion

Overall, carbon nanotubes and carbon fibers LBL membranes provide a new fashion to fabricate electrodes for fuel cells. High loading of catalysts without phase segregation of dissimilar materials can be achieved through synthesis route with very uniform and well-distributed nanoparticle on the sidewalls of SWNTs and CFs. Our modified protocol yielded better Pt nanocatalysts with smaller size and better uniformity. With tight connection between platinum nanoparticles and SWNT or CF, the addition of the incorporation with Nafion significantly increases the number of catalysis sites and improves the accessibility to tri-phase boundaries (TPBs). Thickness, material loading, and the structures of the LBL membranes can be well controlled. Through the technique, one can find an extensive percolation network where improved electronic and proton conductivities is highly possible. The performance of fuel cells corporated with LBL electrodes is very promising, and our approach showed much better results than other groups utilizing similar means. The durability study of the LBL electrodes was not established in this project. However, LBL membranes generally have higher mechanical strength and stability than other membranes made from casting or rolling. It's also known that LBL membranes can survive better in higher temperature or extreme acidic or basic environment. All these reasons suggest that carbon LBL membranes are good candidates for new generation of fuel cell electrodes.

Chapter 3

LBL Zeolite-L Membranes as Zeolite-Modified Electrodes

3.1 Introduction

Study of zeolite-modified electrodes (ZMEs) is one of the main subjects in the field of electrochemistry. Murray and his co-workers conducted very detailed and thorough investigation on this topic in the past three decades[92-98]. Zeolites give numerous possibilities to intelligently designing of the surface of traditional electrodes, improving their response by combining the intrinsic properties of the modifier to a selected electrochemical reaction. The development of zeolite-modified electrodes can now be found in an extraordinary wide area of research topics and is still continuously growing in various field of chemistry[99-108]. There are three main reasons why ZMEs are better than conventional electrodes.[109] First, they combine the advantages of ion exchange voltammetry (common to all the electrodes modified with solid ion exchangers) with the unique molecular sieving properties of the zeolites. One can therefore distinguish between the reactants small enough to diffuse freely within the zeolite framework, and those excluded from (or occluded in) the structure, and thus, not directly involved in the mass transport reactions. The second reason is linked to the development of new electroanalytical sensing devices. By combining the attractive properties of zeolites or zeolite-like molecular sieves, such as size selectivity, ion exchange capacity, high thermal

and chemical stability, with the high sensitivity of modern electrochemical techniques, improvements should be observed as compared to the other sensors based on chemically modified electrodes. The third reason for investigating ZMEs is related to their possible use in electrocatalysis. Zeolites attract interest for this application because they offer a selectivity based on the size and shape of the reactants, together with a three-dimensional lattice made of interconnected cages of molecular dimension coming in a variety of support sites for various catalysts.

Zeolite crystals are aluminosilicates that have attracted considerable attention recently[110-116]. These porous inorganic materials are of particular interest for potential and actual applications such as water softeners, catalysts, controlled polymerization and host systems for a variety of photoactive guests due to the presence of suitable and well-defined rigid cavities and channels. They are stable at high temperatures, insoluble in most organic solvents and offer better resistance to extreme experimental conditions than numerous organic polymers commonly employed to modify electrode surfaces. Besides the durability, their possess the ability to provide a three-dimensional network on the surface, discrimination among solution species by selective uptake on the basis of size (and shape) and charge, and enhanced reactivity by performing electrocatalysis in a heterogeneous medium.

Among all zeolite variations, zeolite-L has emerged as new component for artificial antenna devices[117], self-assembly in functional supramolecular systems[118], and even as connecting agents between living organisms[119]. Zeolite-L consists of interlocking

tetrahedrons of silica and alumina, which form unidirectional channels along the *c* axis of the hexagonal crystal structure that contain cations to compensate the negative charge of the alumina framework[120]. Owing to its optically transparent structure and its porosity, with channels that present an opening of 0.71 nm, zeolite L has shown to be a suitable material for supramolecular organization of different kind of molecules[117, 121]. The organization of nano and microcrystals in films gives rise to collective effects that can be used for the design of new functional materials[122]. Various strategies have been followed to achieve organized zeolite crystals in monolayers on different substrates, ultimately leading to the development of covalent bonding procedures such as direct linkage of functionalized zeolites and substrates[123, 124], or by using specific linkers between both systems[125-128]. However, the preparation of films by covalent bonding presents some important drawbacks, including the chemical modification of the crystal surface and time-consuming synthesis demanded. Therefore, suitable non-covalent strategies, based on physical adsorption[129], convective processes[130], Langmuir-Blodgett technique[131], and layer-by-layer assembly[132], can be used to overcome such limitations. Furthermore, it has been shown recently that zeolite monolayers can be micropatterned by microcontact transfer printing[133], and photopattering[134]. All these methodologies are closely dependent on the aspect ratio of the crystals, thus the control of their shapes and sizes is a necessary prerequisite for particular applications[135]. Interestingly, the orientation of zeolite-L nanocrystals on glass plates depends strongly on the shape of the crystals[136]. While cylinder crystals assemble into a vertically oriented monolayer, hexagonal crystals assemble into a horizontally oriented monolayer.

There are circumstances in catalysis field that require homogeneous zeolite membrane, but the zeolite crystals grown on the substrates tend to crack or grow unevenly, making it difficult to use. Therefore, suitable coatings for zeolite systems with the help from polyelectrolytes should endow the crystals with several beneficial properties, such as the possibility of enhanced colloidal stability, suitable hydrophilicity, and the subsequent formation of a submonolayer on the surface of a substrate. Even though some authors have reported several coating methods of zeolite crystals by layer-by-layer assembly[137-139], reports on the formation of well-ordered zeolite layers on substrates have been very limited[132, 140-142]. In this project we proposed a new way to fabricate zeolite-modified electrodes. We utilized the advantages of layer-by-layer assembly method in the manufacturing process and successfully deposited dense and homogeneous layers of zeolite-L nanocrystals onto conducting ITO substrates with controlled thickness. Membrane morphology was studied by electron microscopy. Electrochemical properties of zeolite-L-modified ITO electrodes were then studied by cyclic voltammetry.

3.2 Synthesis of Zeolite-L Nanocrystals

Aerosil K-330 (31% SiO_2) was purchased from Degussa, Aluminum hydroxide (purum, >99%) and potassium hydroxide (Micro Select pellets, >86%) were obtained from Fluka, Sodium hydroxide (pellets FR for analysis, >99%) was purchased from Merck. Throughout all the synthesis doubly distilled water was used. Disk-shaped zeolite L crystals with different sizes were synthesized according to the procedure described in the literature[143]. Typically, calculated amounts of aluminum hydroxide, sodium hydroxide were added to a precise amount of water and refluxed for 3 h at 120ºC. After letting the basic solution cool down to room temperature, a colloidal silica suspension (Ludox) under stirring was added. The final gel is transferred into a vessel and crystallization took place at 160ºC in a rotator oven during several days. The final product was washed several times with boiling water until the pH of the supernatant became natural. Crystals loaded with potassium cations were prepared by ion exchange by suspending the material in an aqueous KNO_3 solution (0.1 M). SEM image of disk-shaped zeolite-L nanocrystals is shown in Figure 3.1(A). Figure 3.1(B) is the structure of zeolite-L frame work. Note the unique through-the-crystal parallel channels in the framework. They have the diameter about 0.71 nm, which is a good size for housing foreign molecules such as dyes or proteins.

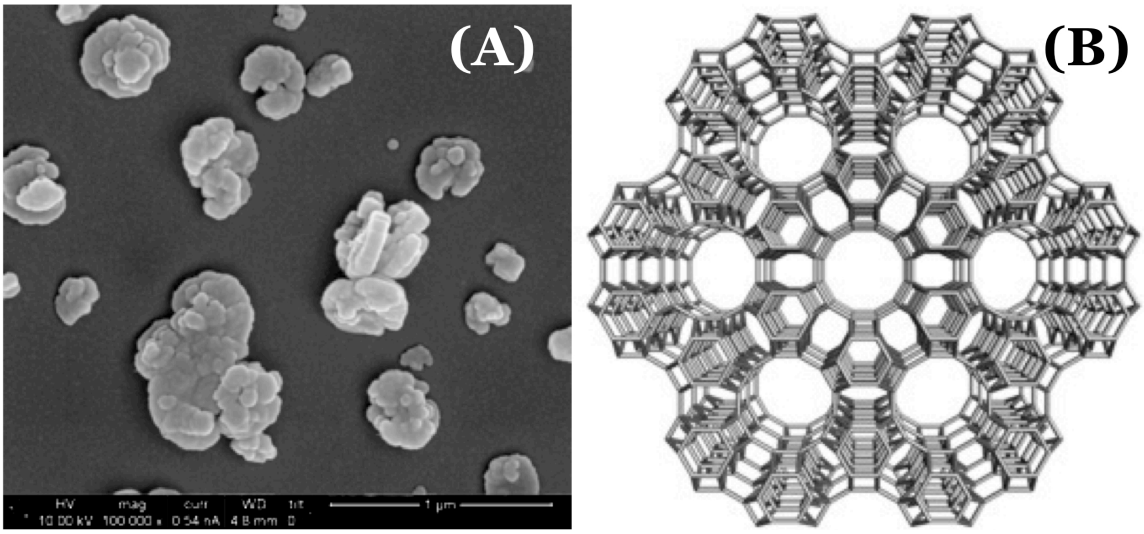

Figure 3.1 (A) As-prepared disk-shaped zeolite-L nanocrystals; (B) Structure of zeolite-L framework.

3.3 Layer-by-Layer Assembly of Zeolite-L Membranes

As-prepared zeolite nanocrystals have negative surface charges from the aluminosilicate framework and the dissociation of potassium cations. To take the advantage of high electrostatic interaction, positively charged polymer PDDA (poly(diallyldimethylammonium chloride), Mw=250K) is chosen as polyelectrolyte in the fabrication of zeolite-L membrane because of the high electrostatic force between PDDA side chains and zeolites. Other polymers such as PEO (poly(ethylene oxide)) and PVA (poly(vinyl alcohol)), which are commonly used in LBL assembly utilizing hydrogen-bonding, are also tested in this study. However, due to the weaker interlayer attraction by hydrogen-bonding and relatively high mass of zeolite nanocrystals, the results are not as successful as PDDA/zeolite pair, hence the investigation is mainly focused on the PDDA and zeolite-L.

Layer-by-layer assembly of of zeolite-L and PDDA was deposited on cleaned glass slides first to study the growth of the film. Glass slides were first cleaned by dipping them in piranha bath (H_2SO_4:H_2O_2=3:1 mixture) for 4 hours. The exceptional hydrophilic surface of the glass slides after piranha treatment directly promotes the adsorption of polyelectrolytes and zeolite-L nanocrystals. Zeolite-L nanocrystals with average diameter of 200-300 nm were dispersed in DI water by sonication for one hour without adding any surfactant or polyelectrolytes. The cleaned glass slides were then alternatively dipped into polyelectrolyte solution and zeolite-L dispersion to form polymer-zeolite bilayers. The cycles can be repeated as many times as possible to make the films reach desired thickness. Rinsing and drying in between each layer of deposition

is crucial. Lack of sufficient rinsing can cause excess polyelectrolytes to enter zeolite dispersion and damage zeolite dispersion. Drying ensures higher adsorption of polymer or zeolite onto the surface.

UV-Visible spectroscopy is used to track the growth of the film and shows perfectly linearly increase on the film thickness after 10 bilayers of deposition (Figure 3.2). The consistent growth rate means the ability of precise thickness control by LBL assembly. SEM images of PDDA/zeolite-L deposited on silicon wafer from one to three bilayers of deposition (Figure 3.3) confirm very steady accumulation of zeolite-L nanocrystals on the surface of the substrate. Although the size and thickness of zeolite-L nanocrystals are not very uniform, they still stack up on top of each other and form parallel-aligned layers. As the number of layers goes higher, some zeolite nanocrystals start to fill in the gaps between already deposited nanocrystals, and some vertically deposited zeolites can be found after 5 bilayers of deposition. In Figure 3.4, one can find the photos of ten and thirty bilayers of PDDA/zeolite-L on clear glass slides. A thick and white-colored film is formed on glass slide with very high uniformity. No cracks or pinholes can be seen by naked eyes. The high thickness and homogeneity of zeolite coating on glass sides suggests very active inter-layer attraction between PDDA and zeolite-L even thought zeolite-L has particle size and weight much higher than PDDA polymer chains.

Figure 3.5 shows SEM images of 30-bilayer PDDA/zeolite-L LBL membrane on glass slide viewing form the top and the cross-section. Although a relatively small

amount of zeolite nanocrystals are vertically deposited, most of the disk-shaped zeolites are sitting flat and parallel to the substrate with aligned c-axis. This is a good indication that the ionic conducting channels inside zeolite nanocrystals are aligned, and active transport through the membranes remains possible. Note that in the cross-section image some vertically deposited zeolite nanocrystals can be seen in the front. This is the result from the cutting and breaking the sample for imaging purpose. Most of the nanocrystals remain well aligned.